CCM-80-18

Center for Composite Materials

INTERLAMINAR FLAW PROPAGATION
MODE II

VINCENT DIMONDI

College of Engineering
University of Delaware
Newark, Delaware

*MSG DI4 DROLS PROCESSING - LAST INPUT IGNORED

-- 1 OF 1
-- ***DTIC DOES NOT HAVE THIS ITEM***
-- 1 - AD NUMBER: D433300
-- 5 - CORPORATE AUTHOR: DELAWARE UNIV NEWARK CENTER FOR COMPOSITE
-- MATERIALS
-- 6 - UNCLASSIFIED TITLE: INTERLAMINAR FLAW PROPAGATION MODE II,
--10 - PERSONAL AUTHORS: DIMONDI,V. ;
--11 - REPORT DATE: SEP , 1980
--12 - PAGINATION: 34P
--14 - REPORT NUMBER: CCM-80-18
--20 - REPORT CLASSIFICATION: UNCLASSIFIED
--22 - LIMITATIONS (ALPHA): APPROVED FOR PUBLIC RELEASE; DISTRIBUTION
-- UNLIMITED. AVAILABILITY: CENTER FOR COMPOSITE MATERIALS,
-- UNIVERSITY OF DELAWARE, NEWARK, DE. 19711.
--33 - LIMITATION CODES: 1
--******
-- END OF DISPLAY LIST

-- ((ENTER NEXT COMMAND))

INTERLAMINAR FLAW PROPAGATION

MODE II

By

Vincent DiMondi

Center for Composite Materials
University of Delaware
Newark, Delaware

September 1980

For

Materials Sciences Corporation
Blue Bell, Pennsylvania

Sponsored By

Naval Air Development Center
Warminster, Pennsylvania

Abstract

The behavior of an interlaminar defect in a Hercules AS/3501-6 graphite-epoxy (Gr/E) laminated beam subjected to flexural fatigue was investigated. Interlaminar defects were simulated by various sizes of Teflon disbonds implanted within the beam at the midsurface. Static flexural tests resulted in specimen flexure failure modes while fatigue loading produced stable interlaminar propagation of the defects due to the action of interlaminar shear stresses. Ultrasonic C-scan techniques were used to monitor defect propagation as a function of initial flaw size and the applied amplitude of the sinusoidal fatigue loading. Results are presented as plots of crack length versus number of cycles for each set of test conditions. Specimens which did not fail after 10^6 cycles in fatigue were tested for residual strength. Failure mode and micromechanical aspects of the flaw propagation results are discussed.

Table of Contents

Introduction

Advanced composites are finding increased usage in load-bearing structural applications subjected to fatigue loading conditions. Since the integrity of a composite laminate significantly affects its strength and stiffness performance flaw criticality has become a concern of designers.

Flaws can arise during processing or from service inflicted damage and are usually of two classes, through cracks and interlaminar disbonds. It is the interlaminar flaw which is investigated in this report. Interlaminar flaws result primarily from processing but can be created by impact causing a zone of subsurface delamination.

During flexural loading conditions small areas of delamination act as stress concentrators and crack initiation sites. In many cases structural elements containing flaws are subjected to fatigue loading spectrums. It is important that the effect of flaws on the ultimate strength and the fatigue life of laminates be understood, the so-called "flaw criticality" problem.

The study reported herein was designed to experimentally characterize the effect of interlaminar flaws on the

ultimate strength and fatigue life of thick graphite-epoxy laminates. Teflon defects of varying sizes were implanted at the midplane of 64-ply (0.35 in.) $[0_4/\pm45_2/\pm45_2/0_4]_{2s}$ laminates which were subjected to sinusoidal loading for 10^6 cycles. The flaw propagation characteristics were studied at intervals during the fatigue history using ultrasonic C-scan and photomicrographic techniques. The results are presented as an empirical data base characterizing the effect of flaw size and stress amplitude on interlaminar flaw propagation.

TEST PROGRAM DESIGN

Specimen Configuration

The thick laminated beams of Gr/E were configured as 64-ply laminates with a stacking sequence of $[0_4/\pm 45_2/\pm 45_2/0_4]_{2s}$. Specimens were 10 inches in length, 3.0 inches in width and approximately 0.38 inch in thickness. Teflon disbonds were implanted at the midsurface of the laminates (between plies 32 and 33). A local coordinate system (r, s,t) was assigned to the specimens as shown in Figure 1. The width of the specimen is measured in the r-direction, length in the s-direction and thickness in the t-direction. Note that the origin of the coordinate system is at the geometric center of the specimen.

Loading Configuration

The specimens were placed in simple three-point beam bending. In this mode the in-plane shear stresses are distributed symmetrically about the r,t plane. This allows the installation of two disbonds in each specimen since crack fronts arising from each disbond experience the same stresses and results in obtaining twice as much data from one test specimen. The space between reaction points is 6.0 inches,

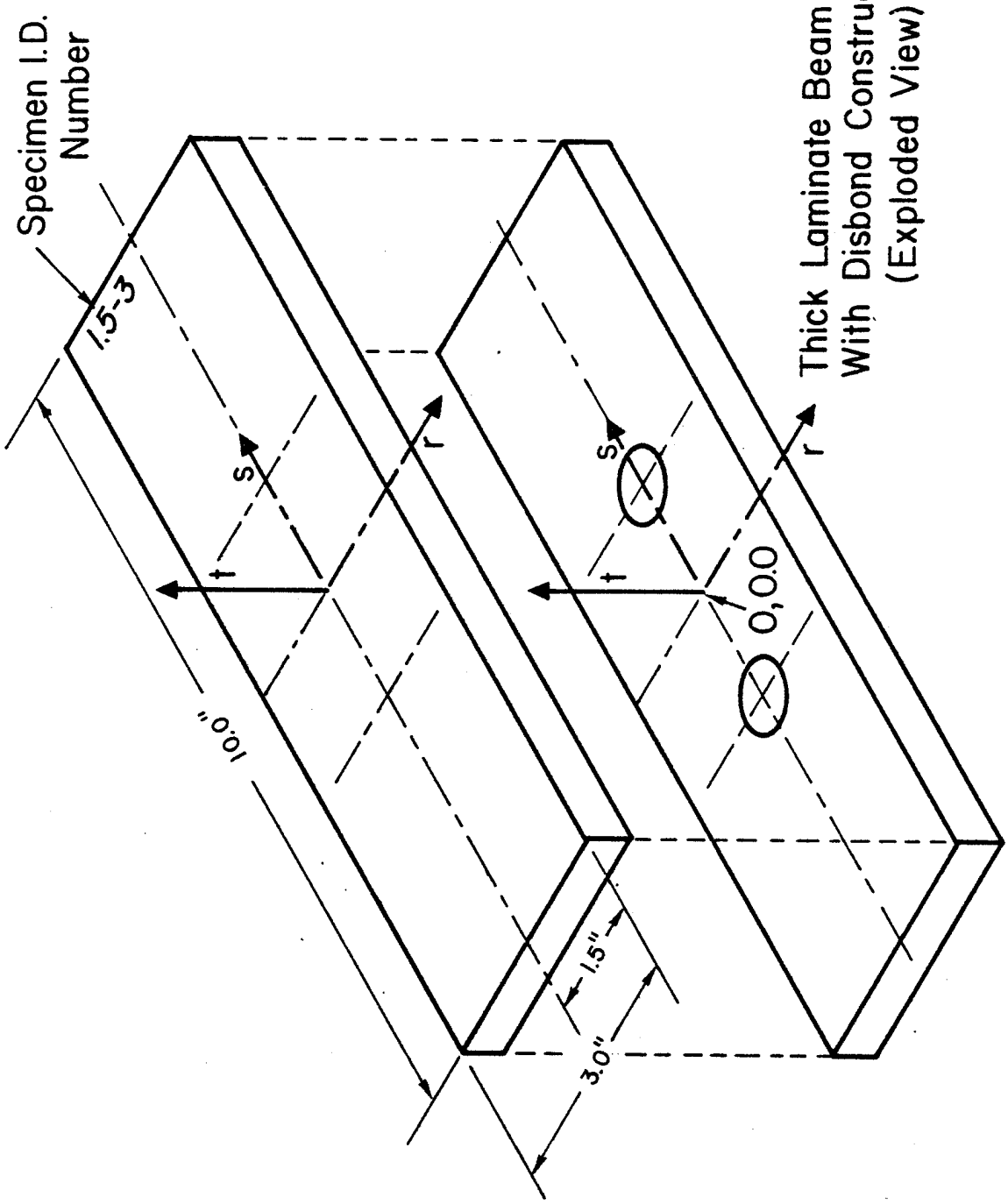

Figure 1 - Thick laminate beam construction

while the load is applied centrally between the two supports (Figure 2).

Flaw Configuration

The Teflon disbonds simulated an interlaminar void due to their two-ply construction which allowed the Teflon surfaces to slide relative to one another. The flaw size was limited to minimize edge effects. Previous studies [1] have concluded that free edges have a definite effect upon the growth of interlaminar cracks. To minimize these effects, flaw widths did not exceed one half of the specimen's width. Criticality of various flaw geometries was examined by using five different sizes and shapes of disbond. These were: 1.0-in., 1.25-in., and 1.5-in. diameter circular; and 1.25-in.×1.0-in., 1.5-in.×1.0-in. elongated flaws (see Figure 3). Note that the elongated disbonds were situated within the beam with the largest dimension parallel to the s-direction. Disbond centers were located along the s-axis either ±1.5 inches or ±2.0 inches from the origin. Each specimen contained two disbonds having the same geometry.

Disbond Fabrication/Installation

The Teflon-Teflon disbonds were constructed from a stock FEP Teflon film 0.001 inch in thickness by doubling the sheet (see Figure 4) and using a steel punch to cut the disbonds.

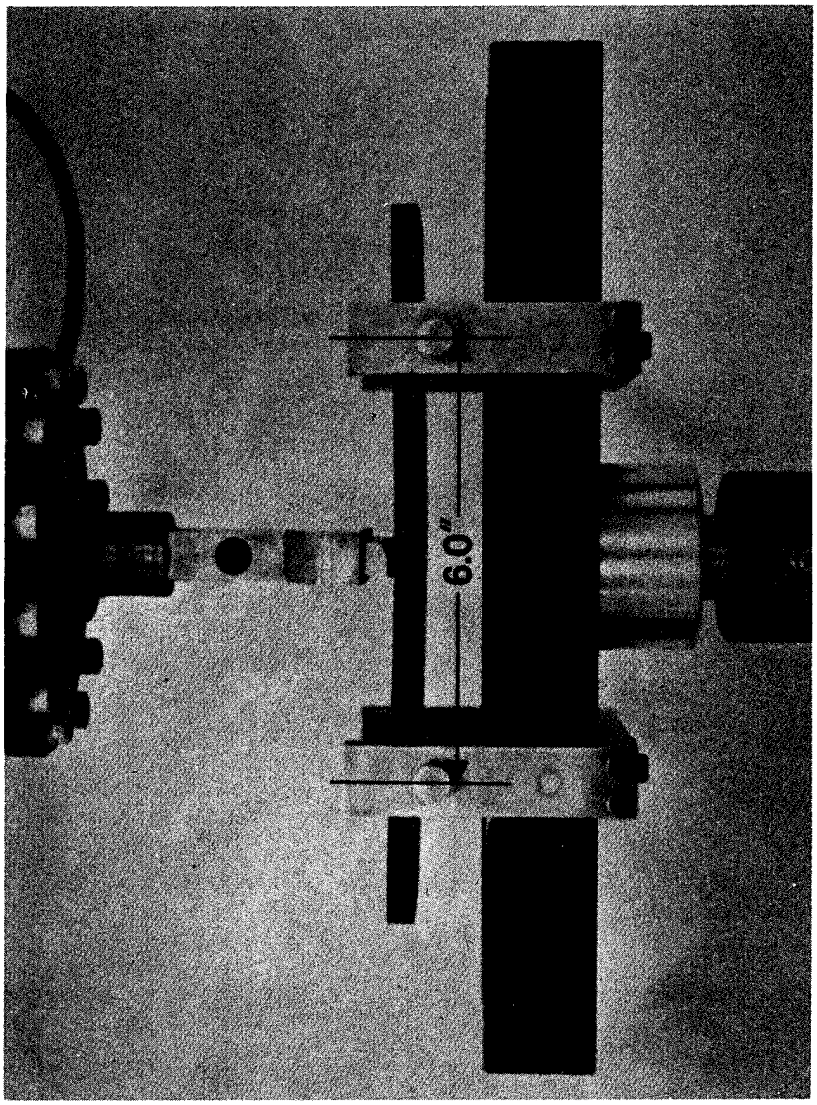

Figure 2 - Thick beam in three point bending

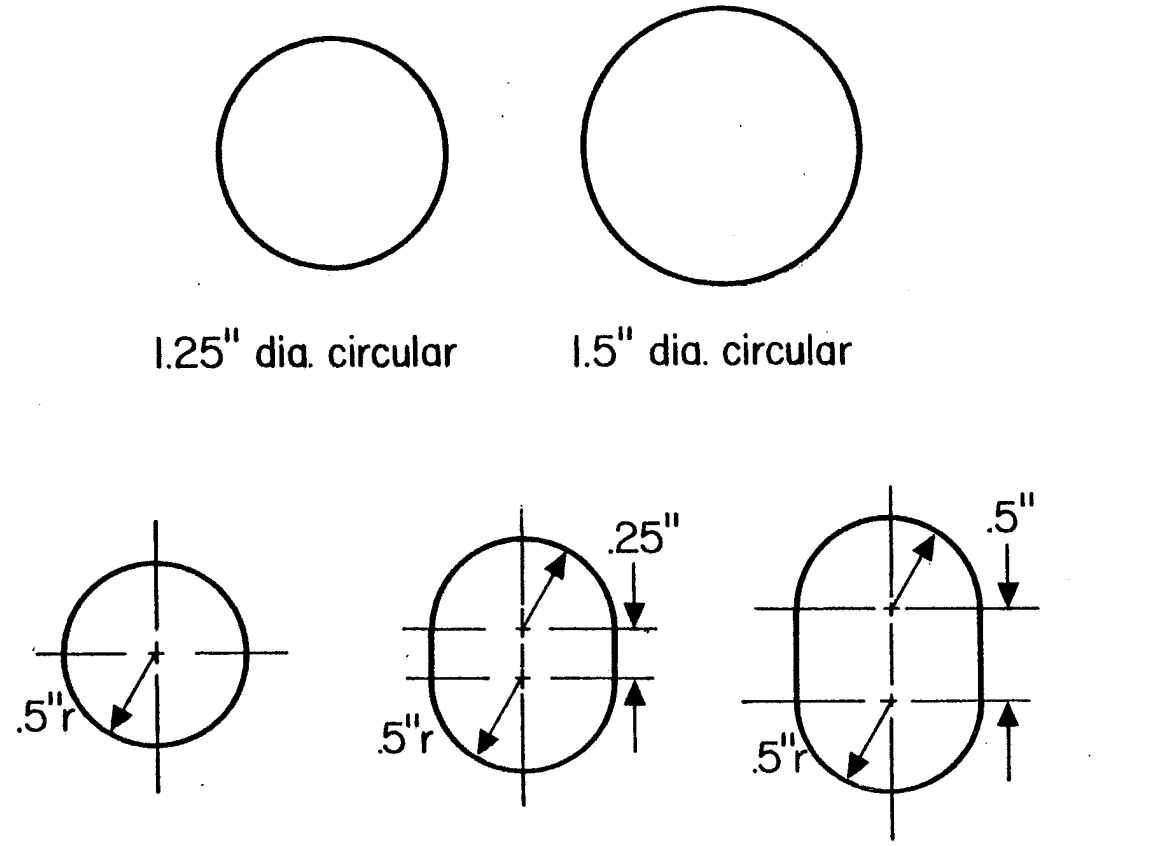

Figure 3 - Disbond geometries

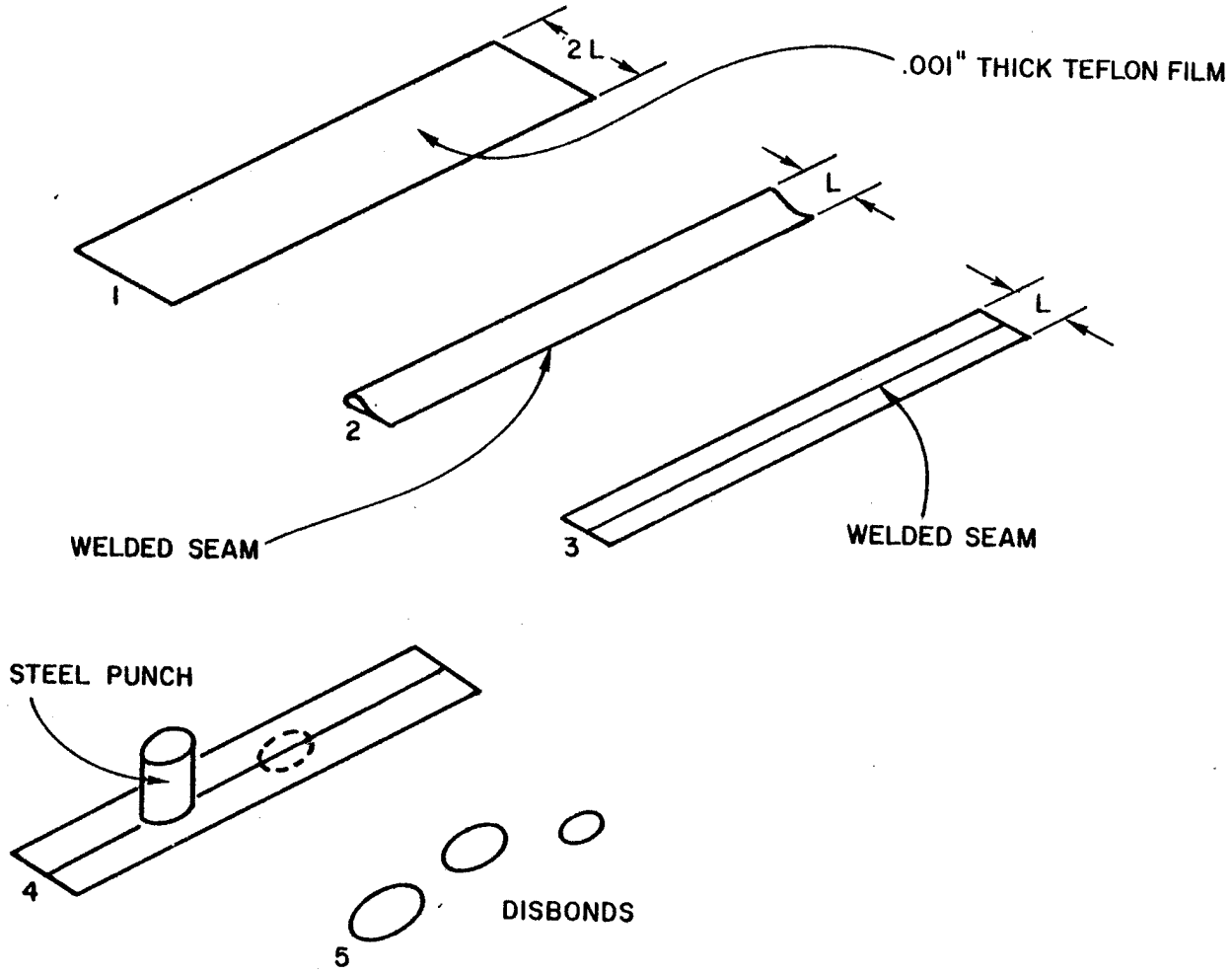

Figure 4 - Disbond fabrication method

The steel punches corresponded in shape to the various disbond geometries.

The laminate was prepared as two identical 32-ply half panels. Disbond installation was facilitated by the use of a Plexiglas template with lines corresponding to the panel edges, and also denoting the placement of the disbonds relative to final specimen edges. Installation of eight disbonds per panel was performed by arranging the disbonds on the template, and placing the template/disbond assembly onto a half panel. The two half panels were assembled into one 64-ply laminate and processed in an autoclave per Hercules specifications.

Specimen Preparation

Hercules AS1/3501-6A graphite-epoxy material in the form of 12-inch wide pre-preg tape was laminated into panels measuring 14 inches in width by 14 inches in length. Each panel was assembled from two half panels of 32 plies each having the stacking sequence $[0_4/\pm 45_2/\pm 45_2/0_4]_s$. Four specimens were obtained from each processed panel. Specimen layout within the panel is shown in Figure 5. After being processed, the panel was inspected ultrasonically to check laminate integrity and determine the exact location of the specimens within the processed panel. Individual specimens were cut from the panel using a diamond impregnated saw.

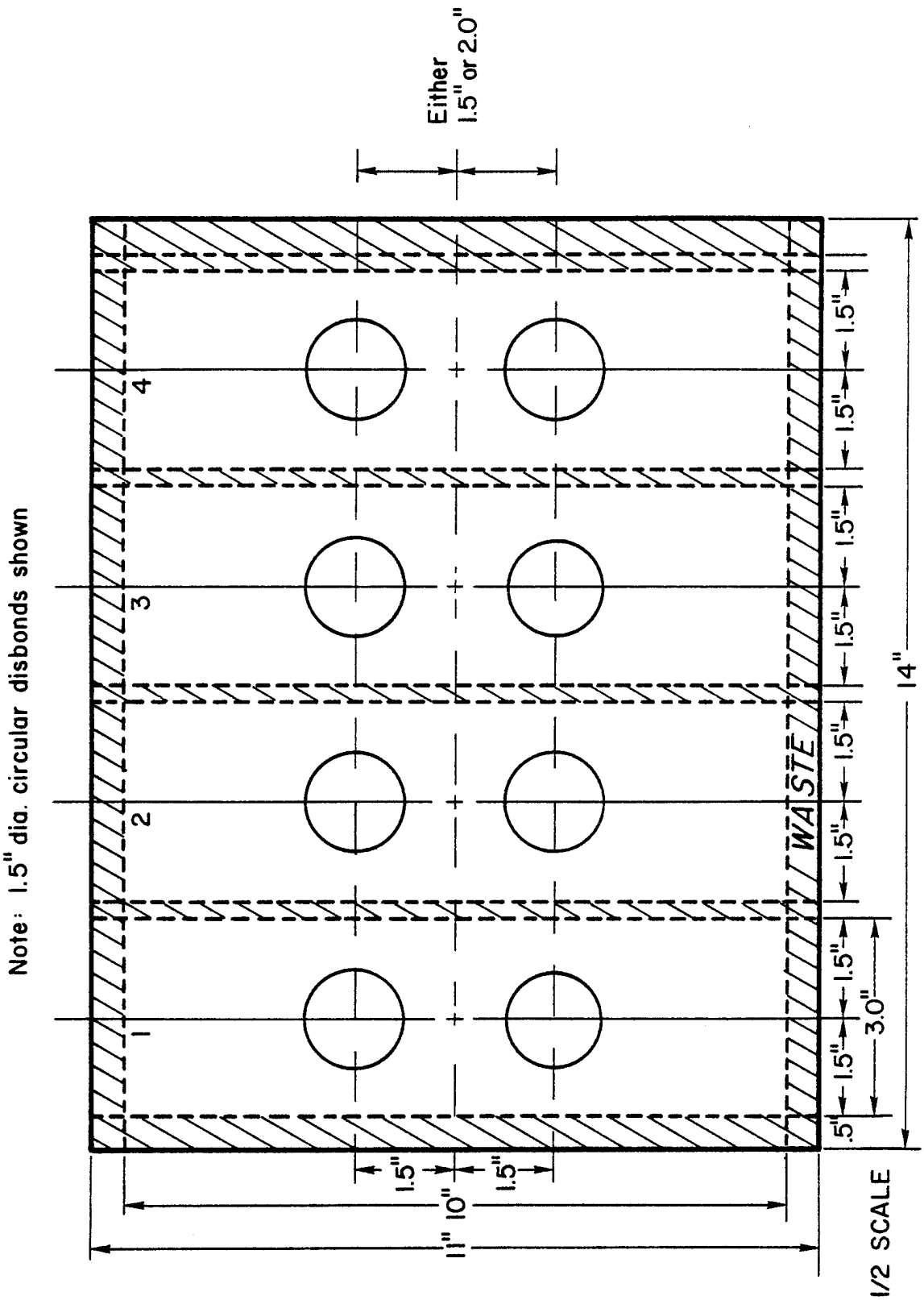

Figure 5 - Processed panel layout

Test Fixture Description

The thick laminated beams were tested in a three-point bending fixture, shown in Figure 6. The 0.375-inch round steel load reaction pins (1) served to transmit a point loading across the beam's width. Support arms (2) (Figure 7) were rigidly connected to the main frame rail (3). During preliminary tests the 0.375-inch loading nose (1) caused localized delaminations and surface damage which was corrected by inserting a $\frac{1}{2}$-in.×3-in.×$\frac{1}{8}$-in. copper pad (4) between the steel nose and specimen surface.

Test Procedure

The previously described three-point bending fixture was used in both the static and fatigue testing of the thick beams. Static tests were conducted in an Instron model TTCML Universal testing machine using a crosshead speed of 0.05 cm/min. Failure was determined as the maximum load recorded on the load deflection curve.

Fatigue loading was performed in an Instron model 1321 servo-hydraulic test frame. Sinusoidal loading was applied at a frequency of 10 Hz in load control with a minimum to maximum stress amplitude ratio of 0.1. The test duration was nominally 10^6 cycles with periodic monitoring of the flaw propagation at selected intervals during the load history.

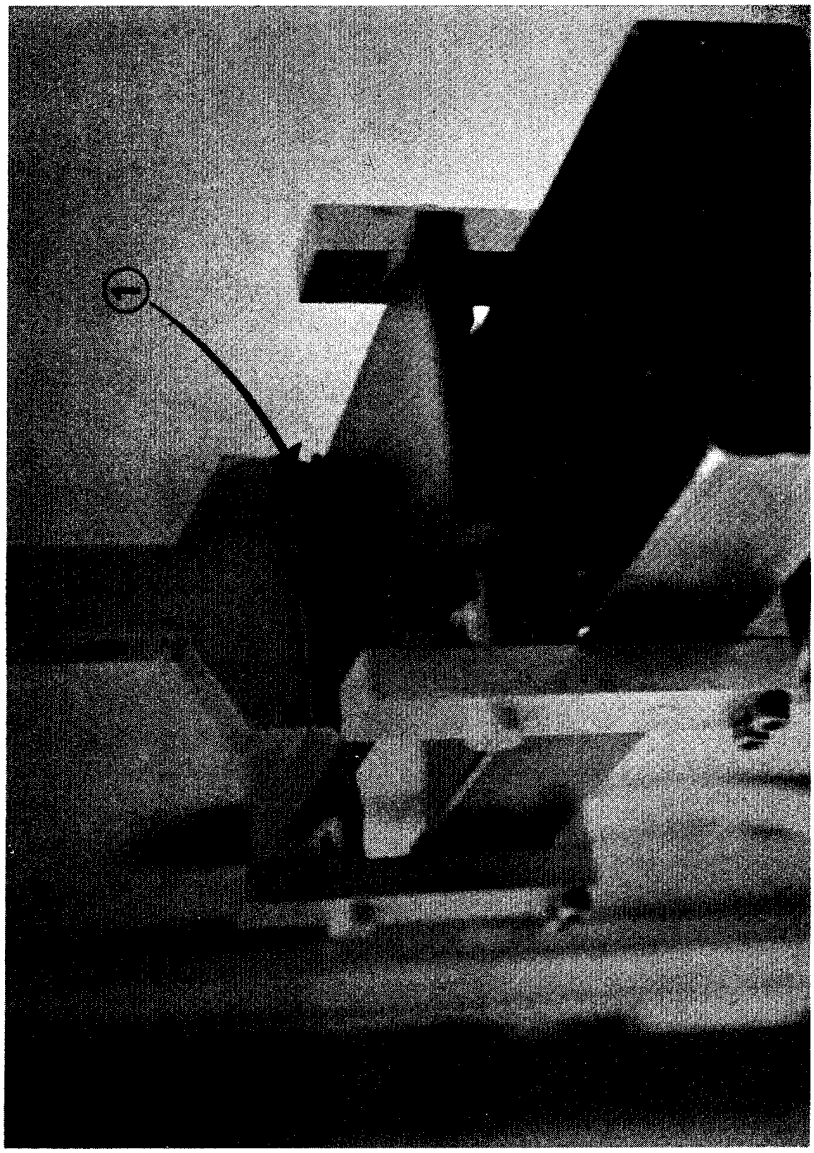

Figure 6 - Test fixture

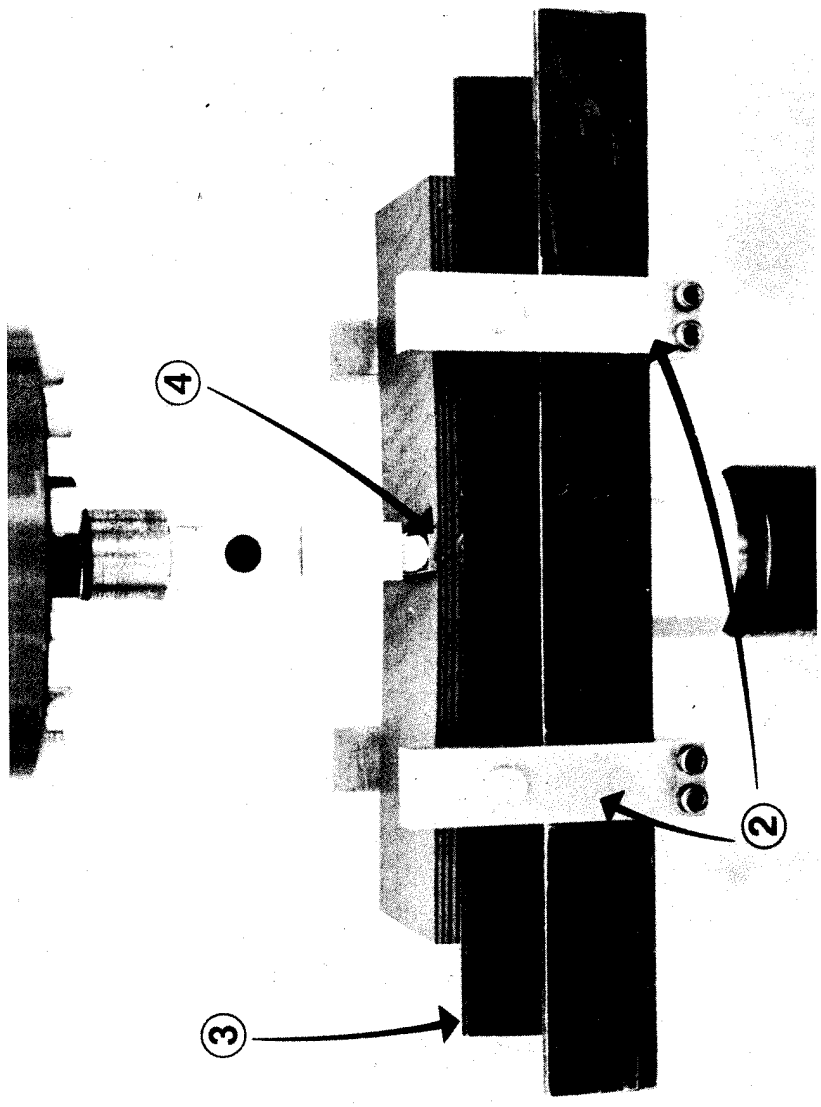

Figure 7 - Test fixture components

Prior to testings, specimens were ultrasonically C-scanned to provide initial flaw measurements and locate the midpoint between the two disbonds. A line was marked on each beam corresponding to the center of the span. The specimen was fatigue tested for an interval, then C-scanned. During Phase I intervals of 5,000 to 10,000 were employed. In this phase, little was known about the rate of crack growth, so care was taken not to use too large an interval for fear of not obtaining growth data. Once a feel for the growth characteristics was obtained, appropriate test intervals were used to expedite testing, based on disbond size and S-level. Once propagation of the defect occurred, intervals were reduced to further characterize flaw growth. Termination of a test occurred when the flaw failed to propagate despite continued cycling, or when the specimen failed through catastropic crack propagation.

Pulse echo ultrasonic inspection was used to nondestructively monitor the flaw propagation during the tests. The ultrasonic system consists of a model 5052 Panametrics ultrasonic analyzer, Tektran tank with scanner and hot pen recorder, and a Tektronix dual trace oscilloscope. The gated peak detector section of the ultrasonic analyzer was used to select the portion of the waveform corresponding to the implanted defects enabling the study to focus on damage propagation from the implanted flaws.

Testing Program Phases

The testing program consisted of three phases. In Phase I specimens containing 1.0-inch circular, 1.25-inch oblong and 1.5-inch oblong disbonds were tested for static strength. Using the strength results, stress levels (S-levels) were determined for the fatigue tests. Fatigue tests in this phase were conducted at S-levels of 40, 50 and 60 percent of the maximum failure load. Disbonds were located ±1.5 inches from origin of the r,s,t plane.

Phase II consisted of 1.25-inch and 1.5-inch diameter circular flaws with centers located at ±1.5 inches, tested at S-levels of 50 and 60 percent of the static ultimate strength. Phase III had 1.0-inch, 1.25-inch and 1.5-inch diameter circular disbonds located ±2.0 inches from the origin in specimens that were tested at S-levels of 50 and 60 percent (except for the 1.5-inch specimens, which were only tested at 50 percent).

TEST PROGRAM RESULTS

Static Test Results

The results of the static tests were primarily utilized in the determination of the stress levels used in the fatigue program. The data is presented in Table 1. Results of static tests performed on the 1.0-inch circular, 1.25-in.×1.0-in. oblong, and 1.5-in.×1.0-in. oblong disbonds indicate an average failure load of 6,920 pounds. All specimens first failed in flexure, the subsequently failed in shear (see Figures 8, 9 and 10). Observation of specimen failures indicate tensile failure of ±45° plies adjacent to the outer 0° plies (plies 59 - 60). This led to subsequent failure of the 0° plies. Additional loading of the specimen caused the specimen to fail in shear.

The experimental results can be compared to results obtained through a laminate analysis routine. The laminate analysis program, CMAP-2, developed by R. C. Wetherhold [2], employs the Tsai-Wu biaxial strength criterion to compute failure of a laminate based on a single ply failure. This approach only predicts failure due to mechanical or thermal loadings in an unflawed specimen. To take into account the

Table 1.

Laminated Beam Static Test Results

$[[0_4/\pm45_2/\pm45_2/0_4]_s]_s$

Width = 76.2 mm, Thickness = 9.6 mm

Specimen No.	Defect Size (mm/in.)		Failure Load (lbs.)
1-1	25.4/1.0		5,690
1-2	25.4/1.0		6,600
1-11	25.4/1.0		8,260
1-13	25.4/1.0		6,830
1.25-1	31.8/1.25		7,820
1.25-2	31.8/1.25		7,260
1.5-2	38.1/1.5		6,830
1.5-4*	38.1/1.5		6,000
		Average	6,920

*Note: failed in interlaminar shear

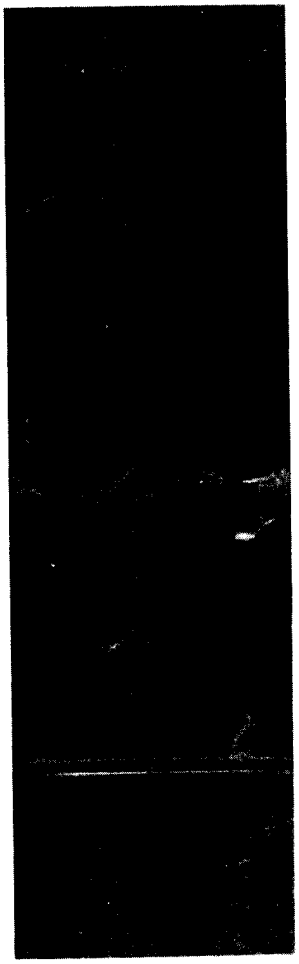

Figure 8 - Statically tested specimen
Flexural failure

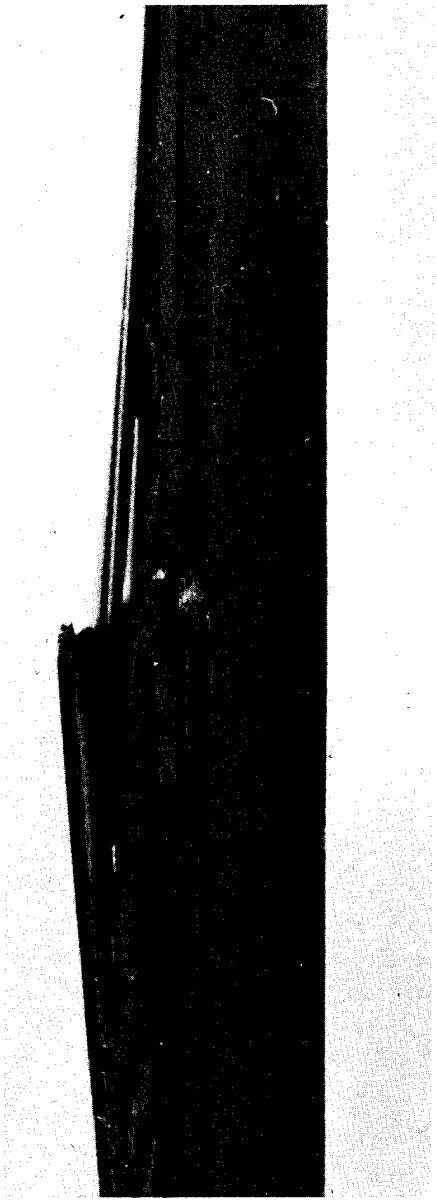

Figure 9 - Static tensile failure - side view

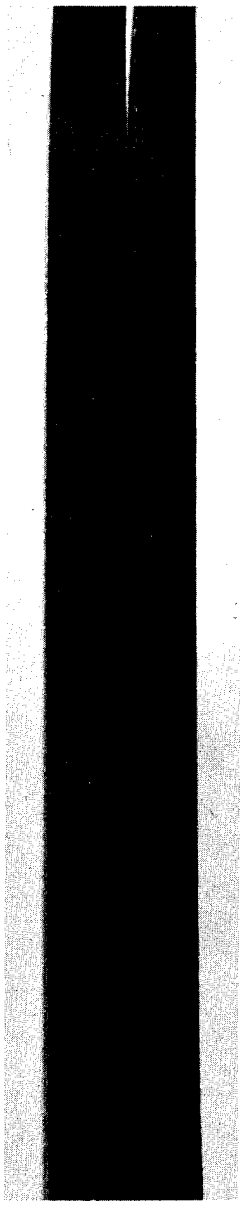

Figure 10 - Static interlaminar shear failure - end view

effect of an interlaminar disbond on laminate failure, a more sophisticated approach such as the one developed by Chatterjee [3] can be used. In this study, however, results showed that static failures occurred in the form of flexural failure of the beam's tensile plies; consequently the interlaminar crack did not effect the results. Therefore, the laminate analysis prediction was expected to be valud due to the similarities in failure modes observed in this experiment and modeled in the laminate analysis.

The laminate analysis program CMAP-2 provided a prediction of 7,270 pounds compared to the experimental average of 6,920 pounds -- a 5% difference. Furthermore, the analysis predicted first failure in the ±45° plies (plies 59 - 60).

Fatigue Test Results

The series of ultrasonic C-scans for each specimen formed a complete chronological history of flaw propagation during fatigue. The C-scan images were a one-to-one image of the actual specimen and flaw. Measurement of successive flaw lengths were recorded from the series of scans. These measurements of crack length at a given number of stress cycles were plotted for the specimen's entire history. Graphics of crack length "a" in millimeters versus cumulative number of cycles were the result of the data obtained

in these experiments. The data obtained from the fatigue testing program were compiled and produced as tables and graphs of crack length versus cycles.

Two disbonds in each specimen gave rise to four crack fronts. Disbond I was the upper disbond (nearest the I.D. number), II the lower disbond. A and B were symbols used to denote the upper and lower halves of disbonds I and II respectively. Likewise, C and D denoted the upper and lower halves of disbond II (see Figure 11). These four disbond halves A, B, C and D initiated the four crack fronts. Measurements of crack lengths were taken at three points along each crack front (locations 1, 2 and 3 in the figure). These measurement locations were independent of disbond geometry or load level.

A measuring overlay was constructed to aid in the measurements. The overlay was fabricated from a sheet of clear acetate film, scribed with lines to conform to the outer edges of specimens. Within these specimen borders, measurement location lines were inscribed extending in the s-direction from locations of $r = -\frac{3}{8}$ in., 0, $+\frac{3}{8}$ in. (Figure 11). To obtain the flaw measurements, the overlay was placed over a C-scan and the overlay borders aligned with the edges of the specimen's image on the scan.

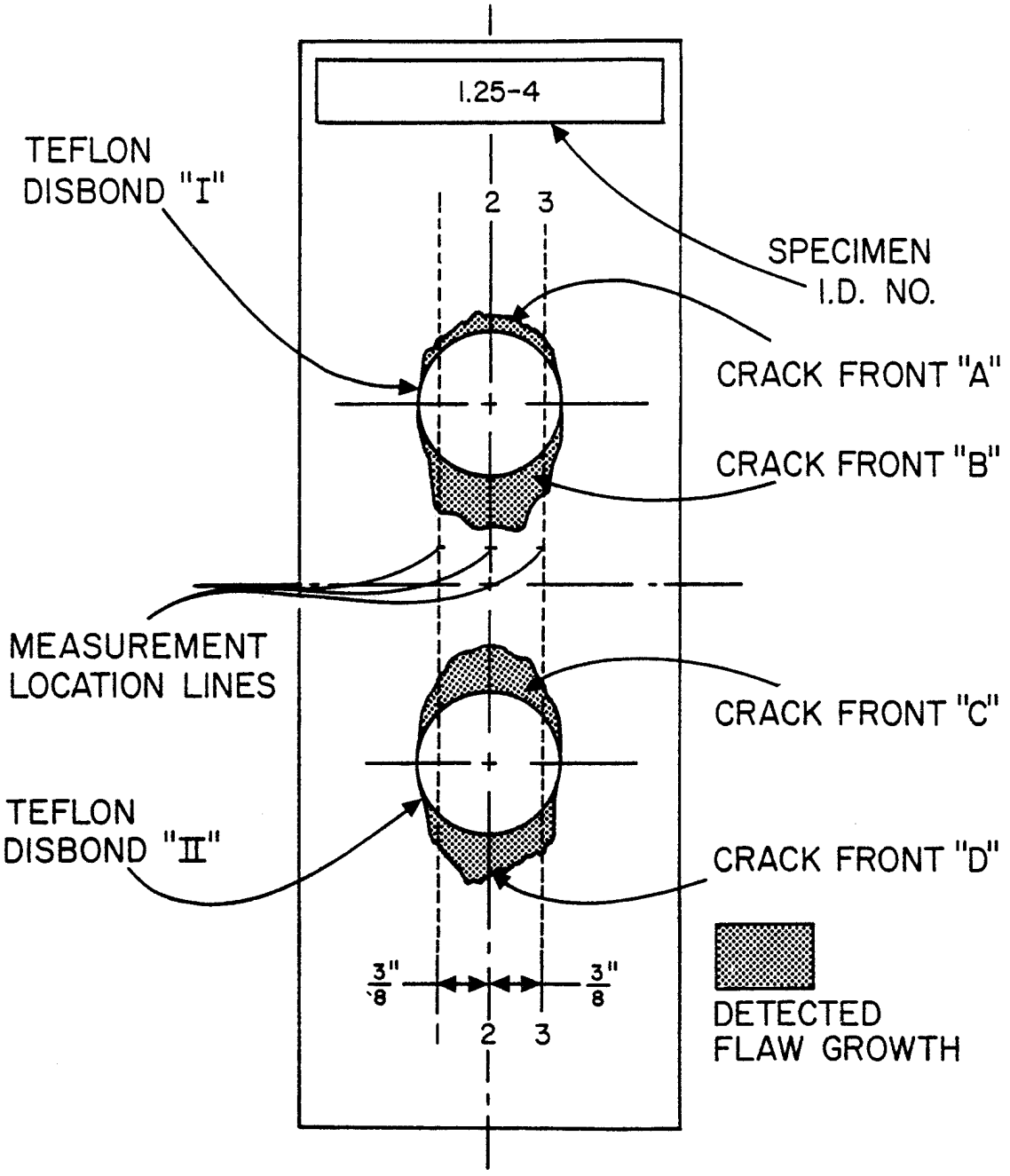

Figure 11 - Crack front locations

Once the overlay was in place, crack length measurements were performed in the following steps:

1. The distance from the top edge of the specimen's C-scan to the intersection of the measuring line 1 with the crack front A were recorded in millimeters.

2. Step 1 repeated for the other two measuring points (2 and 3).

3. The above steps 1 and 2 were repeated for each of the other three crack fronts B, C and D.

4. For each disbond the center of the disbond was computed as follows:

   a. Distances at the two points on the same measuring lines associated with each disbond were averaged to determine the midpoint between the disbond halves.

   b. These midpoint measurements were taken from C-scans of specimens prior to fatigue testing in order to obtain the initial crack lengths.

5. Continue to measure distances as described in step 1 for successive C-scans that show crack growth. Record the distances.

6. Subtract measurements of distances from step 5 from the averaged midpoint distance, found in step 4a, to obtain crack lengths.

The crack length data as a function of fatigue cycles was presented in the form of tables containing crack length measurements at three points along one crack front (note crack front letter in title of table). This data was also presented in the form of graphs. The data was plotted as crack length in millimeters versus fatigue cycles. Note

that both scales varied from specimen to specimen. Horizontal lines at 38 millimeters and 51 millimeters appear on graphs of crack fronts B and C for each specimen. These lines indicate that these two crack fronts propagated only to the center of the beam before the two coalesce.

APPENDIX A

Specimen Identification System

Specimens were identified according to the size, shape and location of the disbonds within them. The system employed in identifying specimens is shown in Figure A-1. The size, shape and location are the first three components of the I.D. scheme. The last two digits indicate the sequence number and crack front location, respectively. The size of the disbond is given in inches; i.e., 1.0 = 1.0 inch, 1.25 = 1.25 inches, etc. The shape and location were denoted by "C" for circular disbonds located at $s = \pm 1.5$ inches, and "C2" for a circular disbond located at $s = \pm 2.0$ inches. As an example: 1.0C2-3. This specimen contained 1.0-inch circular disbonds located ±2.0 inches from the midpoint of the beam. It was the third sample of this type.

Exceptions to this scheme were the specimens tested in Phase I. In this group, both the shape and location symbols were deleted. Consequently, specimen No. 1.25-4 contained 1.25-in.×1.0-in. oblong disbonds located at $s = \pm 1.5$ inches. All specimens in this phase had disbonds located at $s = \pm 1.5$ inches.

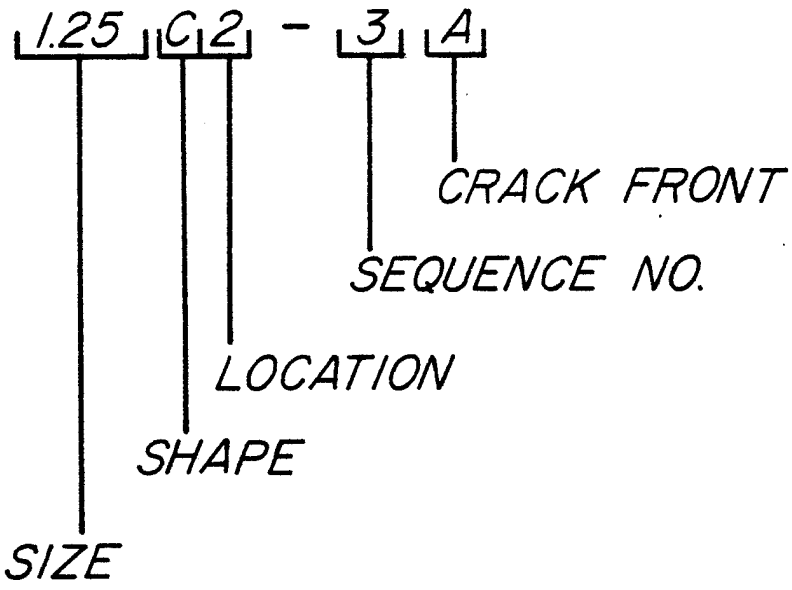

Figure A-1 - Specimen I.D. Schematic

The sequency number was used to distinguish between beams having similar disbond geometries. In addition, this number indicates the location of the specimen within its processing panel. The specimen's I.D. number was scribed on the upper surface of each beam near the top (see Table A-1).

Table A-1.

Specimen No. $[[0_4/ 45_2/ 45_2/0_4]_s]_s$	Defect Size/Shape/Location (in.) (in.)	S-Level	Total Cycles Tested
1-17	1.0/C/1.5	.4	< 625,000
1-18	1.0/C/1.5	.4	<1,075,000
1.25-5	1.25/O/1.5	.4	<1,000,000
	1.25/O/1.5	.4	< 725,000
1.5-5	1.5/O/1.5	.4	135,000
1.5-6	1.5/O/1.5	.4	115,000
1-14	1.0/C/1.5	.5	180,000
1-15	1.0/C/1.5	.5	130,000
1.25-3	1.25/O/1.5	.5	50,000
1.25-4	1.25/O/1.5	.5	100,000
1.5-1	1.5/O/1.5	.5	27,500
1.5-3	1.5/O/1.5	.5	25,000
1-19	1.0/C/1.5	.6	32,000
1-20	1.0/C/1.5	.6	12,170
1.25-7	1.25/O/1.5	.6	11,500
1.25-8	1.25/O/1.5	.6	11,000
1.5-7	1.5/O/1.5	.6	13,000
1.5-8	1.5/O/1.5	.6	16,000
1.25C-1	1.25/C/1.5	.5	60,000
1.25C-2	1.25/C/1.5	.5	33,500
1.5C-1	1.5/C/1.5	.5	10,000
1.5C-2	1.5/C/1.5	.5	22,000
1.25C-3	1.25/C/1.5	.6	6,870
1.25C-4	1.25/C/1.5	.6	15,000

/continued next page

(Table A-1, continued)

Specimen No. $[[0_4/\pm45_2/\pm45_2/0_4]_s]_s$	Defect Size/Shape/Location (in.) (in.)	S-Level	Total Cycles Tested
1.5C-3	1.5/C/1.5	.6	8,880
1.5C-4	1.5/C/1.5	.6	4,150
1.0C2-1	1.0/C/2.0	.5	700,000
1.0C2-2	1.0/C/2.0	.5	328,700
1.25C2-1	1.25/C/2.0	.5	118,000
1.25C2-2	1.25/C/2.0	.5	56,000
1.5C2-1	1.5/C/2.0	.5	19,840
1.5C2-2	1.5/C/2.0	.5	6,750
1.0C2-3	1.0/O/2.0	.6	65,650
1.0C2-4	1.0/O/2.0	.6	117,910
1.25C2-3	1.25/C/2.0	.6	12,580
1.25C2-4	1.25/C/2.0	.6	47,090